Flow around a simplified Car Model (Ahmed Body) – A Case Study

Gagan Jain
Roll No. 180100043
Dept. of Mechanical Engineering
IIT Bombay

Abstract

This report presents a detailed analysis of the research work done for studying the flow around the simplified automotive model called the "Ahmed Body". The introductory section gives an overview of the problem as well as the key motivation for carrying out the study. The next section outlines some of the previous research carried out on the topic. This is followed by looking at the mathematical formulation and computational methods used to study the problem. Finally, we conclude the report with some discussion over some of the ways in which the problem can be approached, other than the already existing research work.

1. Introduction

Aerodynamics of vehicles is crucial from a design perspective and governs the shape of the vehicles. The limited resources of fuel have made it clear that we need to design vehicles that are fuel-economical, along with the constraints of being operationally safe and service accessible. The aerodynamics of a vehicle, along with some other factors plays a crucial role in fuel consumption.

Ground vehicles can be termed as bluff bodies moving in close vicinity of the road surface. The aerodynamic features of ground vehicles are strongly related to some complex interactions between flow separations and strong trailing vortices expanding far in the wake. So, a detailed knowledge of these physical mechanisms is important to be able to design efficient automobile systems.

1.1 Problem Description - The Ahmed Body

Ahmed Body (Ahmed et al.[1]) is a simplified generic car body, with a configuration such that it captures the essential features of a real vehicle flow field. The body consists of three parts: a forebody, a midsection and a rear end (Fig. 1), with the edges of the forebody, rounded to avoid flow separation. The main body is followed by a fully separated region. Some of the features of a real car flow field like due to rotating wheels, engine and passenger compartment flow, rough underside, and surface projections are omitted to keep the analysis simple and focused.

The middle section of the body is a sharp-edged rectangular cross-section. The rear end had the most interesting setup for the experiment; the base slant angle is variable in a range 0^o to 40^o, in steps of 5^o, with the same rear base length. The model is instrumented with pressure taps for measurement.

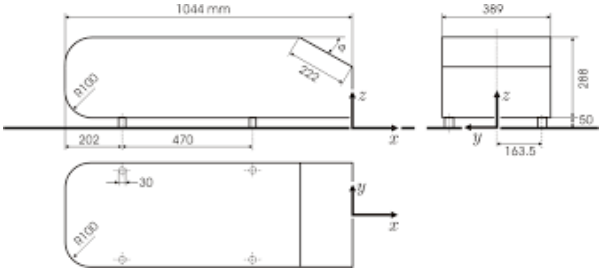

Fig 1: Ahmed Body

Having regions of separated flow is a key feature of the flow field around the vehicle, however simple the design may be. The Ahmed body was designed with the aim of observing a strong three-dimensional displacement flow in front, a relatively uniform flow in the middle, and a large structured wake at the rear. Additionally, vortex shedding, flow reattachment, and recirculation bubbles are also found around the bluff body, which can greatly affect the lift and drag coefficients.

So, the experimental attempt to the problem attempted the following -

- Identify the time-averaged flow structures present in the wake region.
- Analyze the effect of body geometry on wake structure, pressure distribution, and drag.

Another motivation to carry out this experiment was to be able to provide experimental data, which is essential to theoretically model vehicle flow fields.

1.2 CFD Approaches to Ahmed Body

Computational Fluid Dynamics (CFD) has evolved amazingly in the past few years, thanks to the research on mathematical models to represent fluid flows, and the ever-growing access to computational power which made it possible for CFD to become a vital tool in industrial research, development, and investigation.

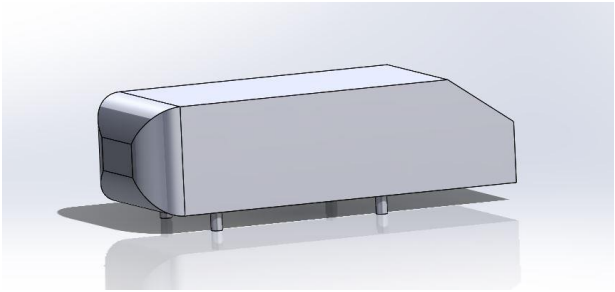

Fig 2: 3D CAD Model of Ahmed Body for CFD Analysis

The experimental study of the Ahmed Body made the data accessible to all and led the foundation of modeling and simulation for vehicle flow fields. The simple geometry of the Ahmed Body (Fig. 2) has made the modeling, meshing, and comparison between experimental and theoretical data quite easy.

There have been several attempts to model the flow behavior, leading to some interesting insights about the nature of turbulent flows. Researchers have approaches like large-eddy simulations (LES), Detached-Eddy Simulations (DES), and Reynolds-Averaged Navier-Stokes (RANS) models. A later section in this report discusses some of these attempts, outlines the models used, and describes how well the results match with the experimental data.

1.3 Applications of the Study

The Ahmed body was created to analyze some of the salient features of the time-averaged ground vehicle wake in 1984 by S.R. Ahmed, and since then, it has become a benchmark for aerodynamic simulation.

New design experiments in the automobile industry look at the experimental results on the Ahmed body to incorporate changes in the vehicle designs. This reference has helped the industry a lot by reducing overall production time, starting from concept through production, by finding and correlating the parameters of drag force, lifts force, yawing moment, pitching moment, and rolling moment of an Ahmed Body, which acts as a representative of a vehicle.

This help has not only been economical but has also provided a competitive edge to industries, which can now put in their time and efforts in researching new technologies, expanding the corporation, or stabilizing product cost to fit the demands of the customers.

1.4 Motivation for studying the problem

Ahmed Body is a simplified version of an actual car body, which enables the investigation of the turbulence behavior of newly developed cars for complex geometry cases. The complexity involved in the automobile design, due to a large number of accessories and devices that form its geometry makes the validation tasks unaffordable. The Ahmed body, on the other hand, retains the main flow features but does not add unnecessary complications so that the problem remains easier to work with.

Although the Ahmed Body is a benchmark model and only the rear slant angle is varied in the experiments, a brief CFD analysis can also show the effects of changing ground clearance and front-end curvature on the total drag. The Ahmed Body analysis also serves as a platform to include additional complex features in the problem, layer-by-layer, to see how the additional complexities change the results, gradually heading one step closer to the real-world cars.

Advancements in vehicle aerodynamics are always greeted by environmentalists and industries equally because such advancements lead to lower fuel consumption and lower carbon dioxide emissions into the atmosphere. In fact, the governments in many countries support continuous aerodynamics improvement programs as a way of mitigating the energy crisis and pollution.

Fig. 3 shows the relation between the power necessary to overcome aerodynamic drag and rolling resistance for a 40 tons truck with the Drag Coefficient equal to 0.5. Clearly, for speeds over 80 km/h, the aerodynamic drag governs the power required. Therefore, it becomes essential to study the aerodynamics of vehicles for efficient design.

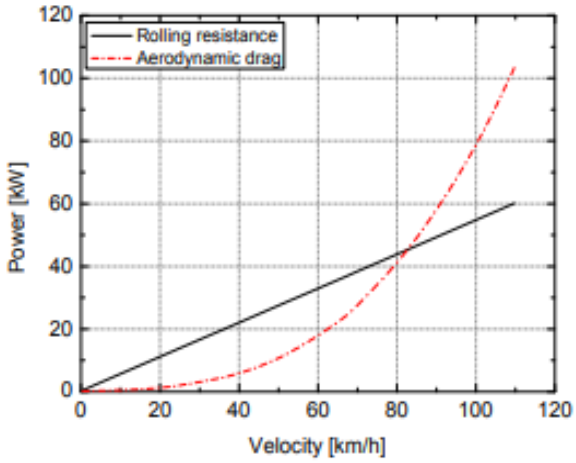

Fig 3: Power needed to overcome drag and rolling resistance for a 40 ton Truck with 0.5 C_d. Source: ICCT (International Council on Clean Transportation)

1.5 Impact of studying the problem

The study of the Ahmed Body problem, instead of benefitting a certain aspect of the automobile industry, has governed the way the whole automobile industry should take steps ahead. The research has not only been an optimizing factor, but also a guide to designing efficient vehicles. The automobile industry today is working on two major aspects revolving around this research work, first is designing vehicles keeping in mind the results from this experiment, and second, carrying out research on more complex geometries which are generalizations of the Ahmed Body design.

Several pieces of research are being carried out on aerodynamics of heavy-duty vehicles using the Ahmed Body analysis as a reference. One such example is the ongoing research at the Experimental Aerodynamics Research Center, in Brazil.

1.6 Objectives of the Study

So, the key objectives of the study are to improve the aerodynamic design of the body, analyzing the flow field to understand the nature of these improvements, and reaching a suitable and reliable experimental-numerical

setup for such a flow. The key effects of the diffuser geometry on the aerodynamic characteristics of the body are also to be analyzed using the flow field around the body. All these aspects build the foundations of how real-world automobiles are manufactured today.

2. Literature Review

The problem has been set up and initially approached from an experimental point of view and the experimental data obtained has served as validation data for computational models.

2.1 The Original Experiment

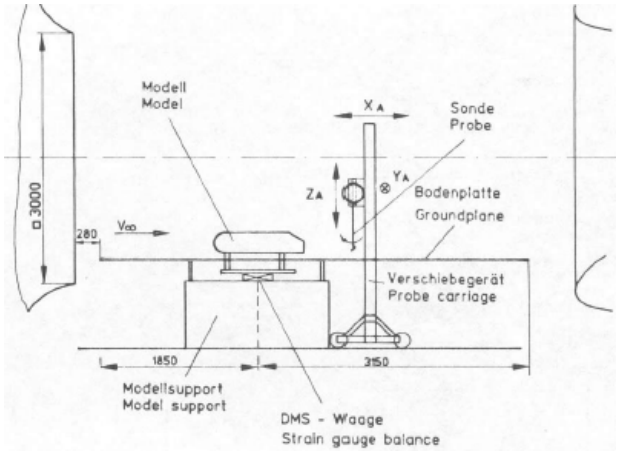

Fig 4: Experimental set-up in a wind tunnel

The introductory section of the report already describes the experimental model for carrying out the analysis. The experiment (Ahmed et al.[1]) was conducted in the DFVLR subsonic wind tunnels for pressure measurements, flow visualizations, wake survey and force measurements. The model was fixed on cylindrical stilts above a ground board with rounded leading edges to avoid any kind of flow separation. All the experiments except the visualization were carried out at a wind speed of 60 m/s, which corresponds to a Reynolds number of 4.29 million.

A. Wake Survey

A ten-hole directional probe, with a conical tip having two pairs of orifices, one sensitive to flow yaw and the other to flow incidence, was employed for the wake survey. For determining the flow angularity, yaw rotations were imposed to equalize the pressure in the yaw sensing orifice pair, with the probe shaft vertical. The pressure difference was used to calculate the local flow incidence.

Similarly, incidence rotations were imposed to equalize the pressure in the incidence sensing orifice pair. In this case, the probe shaft was horizontal. The yaw angle was again determined using a calibration curve as before. The anticipated incidence and yaw flow gradients were used to decide the orifice pair to be used to align the probe.

The mean pressure values measured were functions of local static and total pressure, which were further used to evaluate the static and dynamic pressure, and eventually the magnitude and direction of the local velocity vector. Another orifice was used to detect flow reversal. If the pressure at the rear probe tip exceeded the value sensed at the probe tip, the shaft is rotated 180º.

The movements of the wake survey probe were remote-controlled and the flow angle was measured with estimated accuracy of ±0.4º.

B. Pressure and Force Measurements

These experiments were majorly aimed at checking the flow symmetry with the yawed onset flow in the range of ±10º. The force measurements were done by connecting the model to a strain gauge balance, arranged below the ground plane. The forces and moments were measured with estimated errors of ±0.2 N and ±0.1 Nm respectively.

C. Drag and Pressure Measurements

The total drag values obtained match to a significant extent with previous research works, even though there were evident differences in the model geometry. Contributions to pressure drag from front part c_K^*, slant rear part c_S^*, and vertical rear end base c_B^* were evaluated for various rear-end slant angles by integrating the axial component of the measured pressure over the surface. The obtained numerical values are listed in Table 1.

Base slant angle φ	c_W	c_K^*	c_S^*	c_B^*
5^o	0.231	0.016	0.010	0.158
12.5^o	0.230	0.016	0.037	0.122
30^o (High Drag)	0.378	0.016	0.213	0.092
30^o (Low Drag)	0.260	0.019	0.089	0.101

Table 1: Drag breakdown for three configurations

This clearly indicates a small and almost constant contribution of the forebody c_K^*=0.016, which leads to the conclusion that the inference between the rear end and forebody flow is weak, maybe due to the relatively long midsection and this might not hold well for a body with a short midsection. The major contribution of the pressure drag comes from the slant and vertical base surface of the rear end. For a zero base angle, the rear end pressure is totally contributed by the flat base, and with increasing values of the angle, the vertical base area decreases, but the pressure distribution changes as well, leading to an overlap of geometrical and fluid mechanical effects.

It is important to note that the relative values of pressure drag vary between 76% and 85%, with friction drag accounting for the remaining. The high drag configuration with the rear base slant angle equal to 30^o has 85% of its total drag resulting from pressure drag, thus emphasizing the increasing importance of friction drag for low drag configurations.

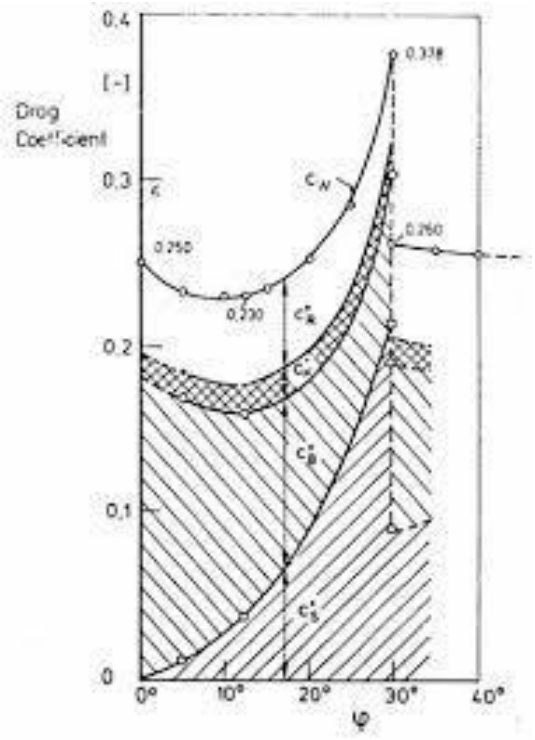

Fig 5: Variation of Drag with base slant angle variation

Strong vortices are present in the flow field of the 30^o rear angle, which influences and governs the flow over the whole slant surface. Low drag flow for the same configuration shows a flow separation at the slant surface.

D. Wake Structure

The time average flow exhibits a macrostructure which appears to govern the pressure drag created at the rear end. The shear layer coming off the slant side edge rolls up into a longitudinal vortex. The shear layers at the top and bottom edges also roll up as shown in Fig. 6. The recirculatory flow regions A and B can be thought of as being generated through two ‘horseshoe’ vortices situated one over the other in the ‘separation bubble’ indicated by D. The ‘trailing’ vortices from the upper and slant side edges merge eventually.

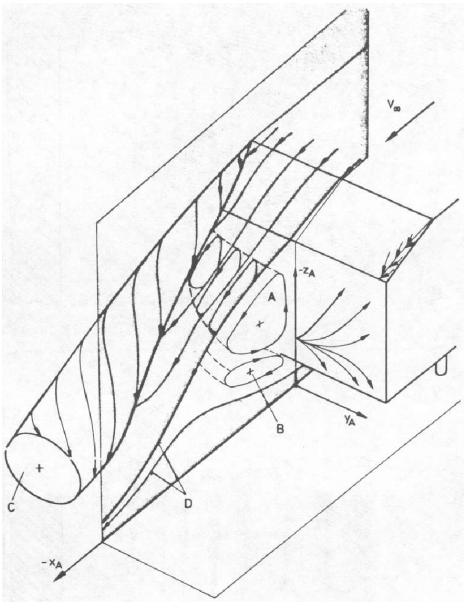

Fig 6: Horseshoe vortex system in the wake

The strength of vortex A as shown in Fig.6 is dependent on the strength of vortex C, as the flow over the slant surface is influenced by it. As long as flow does not separate, the strength of vortex C depends upon the base slant angle. The strength of vortex B is dependent on factors like ground clearance and is indirectly linked to the base slant angle. The upper and lower regions have comparable magnitude for a slant angle of 5°, but the upper region dominates the lower for a slant angle of 25°. The separation bubble length also almost halves as the angle is increased.

A low drag rear end configuration induces a weak transverse flow in its wake. On the other hand, high drag generating flow is characterized by strong side edge vortices, a separation bubble on the base slant surface, and the separation bubble originating from the vertical rear end base. The presence of strong side edge vortices prevents a lateral widening of this separated flow. This high drag flow is unstable, and the switch over to the stable low drag flow is accompanied by the disappearance of strong vertical motion in the wake.

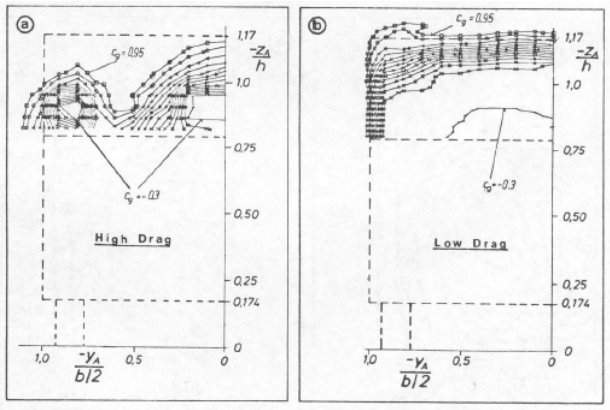

Fig 7: Total Pressure Isobars for base angle = 30^0 for high and low drag cases

It has been experimentally observed that for a rear base slant angle below 30°, formation of side edge vortex with a primary and a secondary vortex formation can be observed. But for angles greater than 30°, the separation region on the slant surface joins the separation bubble of the base, and so the corresponding vortices can no longer be considered as separate. This merging is triggered by seemingly insignificant disturbances in the oncoming flow and leads to the switching over to the low drag flow.

E. Key Conclusions from the Experiment

The major contribution of the total drag comes from the pressure drug, out of which the forebody has less than 10% contribution to the pressure drag. Most of the pressure drag is generated at the rear end of the vehicle.

The rear base slant angle of 30° serves as a threshold for flow separation. As a result, many of the computational approaches, as described briefly in the next sub-section, aimed at modeling the Ahmed Body flow are carried out at the angles 25^0 and 35°, to be able to analyze both kinds of observations.

F. Another Experiment

Linehart et al[2] performed another set of experiments for the same geometry of Ahmed Body, with more focus on flow visualization, hot wire and LDA measurements for two different rear slant angles: 25º and 35º, which bracket the critical instability when the flow detaches from the slanted surface. LDA measurements include all three components of mean and RMS velocity as well as most second and third-order moments.

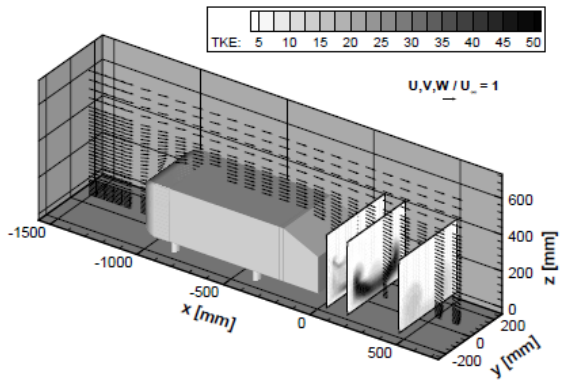

Fig 8: Velocity Distribution and TKE for 25º angle[2]

The differences in flow attachment and recirculation are pretty clear from these experiments and certainly helped in a lot of computational studies that followed, thanks to the technological advancements which happened in the course of time. Fig. 8 shows the overview of velocity distribution and turbulent kinetic energy around the 25º slant Ahmed Body.

2.2 Computational Studies

There have been several attempts to model the flow over the Ahmed Body, using different methods, some of which are described in this section.

Gillieron and Chometon[3] compare the simulated values of aerodynamic drag coefficient and vortex wake flows at different values of rear base slant angles. They used classical numerical schemes and default relaxation values for the continuity and momentum equations and carried out the computation assuming stationary flow, incompressible fluid conditions, and uniform inlet velocity. The computed aerodynamic drag coefficient reported was higher than the experimental ones but showed the same basic pattern for variations in the rear slant angle, as shown in Fig. 9. The results also indicate the changes in vortex wake airflows. The critical angles, at which the transitions from 2D base behavior to 3D hatchback behavior and back to 2D base behavior occur, correlate well with the experiments.

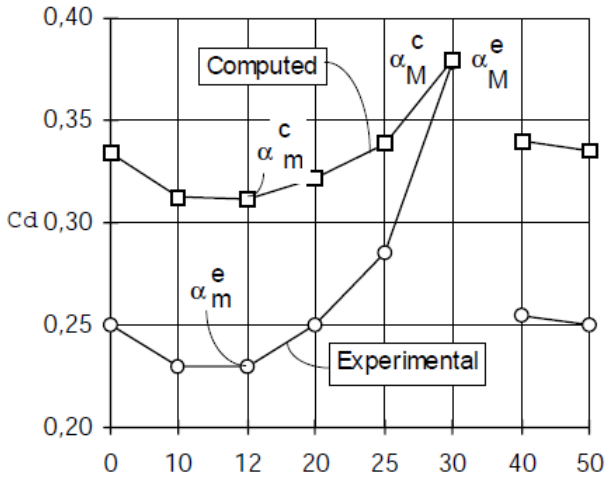

Fig 9: Computed Aerodynamic Drag Coefficient by Gillieron and Chometon[3]

Howard and Pourquie[4] presented the first large eddy simulation (LES) of the Ahmed reference model and analyzed a wide range of flow results: time-averaged mean profiles, time-dependent traces, flow spectra and a number of 2D and 3D animations of the model for a rear base slant angle of 28^0. They solved the incompressible Navier-Stokes equation using an unstructured tetrahedral method for appropriately chosen domain dimensions. The level of Reynolds number required a log law method to calculate the velocity at the first near-wall grid point, which was done

iteratively. The pressure coefficient at the edge where the top surface is cut away indicated the presence of the separation generated over the sloping surface.

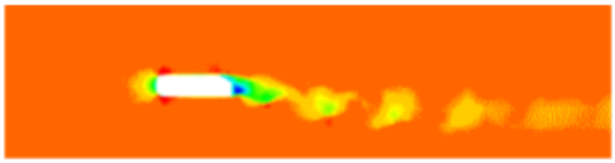

Fig 10: Stream-wise velocity with range variation -0.5L/s < u < 1.2L/s by Howard and Pourquie[4]

The streamwise velocity flow is as shown in Fig. 10, which has a stagnation point at the center of the front face, and the flow remains attached as it passes across the flat top, bottom, and side surfaces of the body. The drag coefficient was calculated to be around 0.25, which was quite close to the values obtained in the experiment for angles above 30°. The relative contributions of drag from various parts of the body also agreed to a good enough extent with the experimentally obtained values, except for the fact that the modified log law predicted a higher surface shear stress for the same near-wall velocity value for the front end of the body. The mixing layer due to separation generated span-wise vortices which fed into the horseshoe vortices. The two recirculating regions interacted with each other and the unsteady flow coming from the two surfaces hence remained separated. This indicated that the flow produced in this work was in the post-critical-angle regime rather than the pre-critical one. The paper, as a concluding remark, stressed upon the need to carry out further simulations at various slope angles to confirm these observations and make them more accurate.

S. Kapadia et al.[5] presented a Spalart-Allmaras based detached eddy simulation (DES) hybrid model and numerical results for a 25° base slant angle using Cobalt, a parallel, implicit, unstructured Euler/Navier-Stokes flow solver, which works on the principle of Godunov's first-order accurate, exact Riemann method. The paper also compares the different turbulent models in terms of accuracy and cost. The S-A model solves a single partial differential equation for a variable that is related to the turbulent viscosity. The DES simulations are put to work in a way in which the model acts as an S-A RANS model near the wall surfaces and as a sub-grid LES model away from the wall. The numerical solver uses discretization to solve the equations.

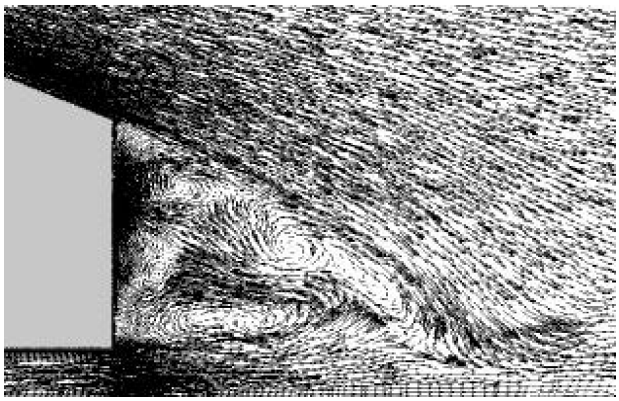

Fig 11: Wake flow structure at the plane Z=50mm by S. Kapadia et al.[5]

The flow pattern obtained shows similarities to the flow described by Ahmed et al.[1]. The existence of localized circulatory regions (Fig. 11) suggests that a large part of flow energy is present in vortices. It also fits in the 3-D range of hatchback flow described by Gillieron and Chometon[3] for the lower and upper critical angles of 12° and 30° degrees respectively. The counter-rotating dipolar vortices form a quadruple. The Mach number is less near the frontal area and it is maximal in the wake region, as expected. The pressure contours are similar to those observed by Howard and Pourique[4] who used the LES turbulence model.

After a little fluctuation in the drag values for approximately 3 seconds, C_d approaches a constant value for both DES and

RANS. The average value of C_d for DES is 0.2585 (which matches to a good extent with Ahmed et al.[1]) and for RANS is 0.3272 (which depicts a similarity with the result obtained by Gillieron and Chometon[3]).

Another recent attempt worth considering was by Guilmineau et al.[6], who presented numerical simulations for the prediction of the flow around the Ahmed Body, with the 25° and 35° slant angles, obtained with the flow solver ISIS-CFD. A RANS turbulence model, as EARSM (Explicit Algebraic Stress Model) and two hybrid RANS-LES models, as DES and IDDES (Improved Delay DES) models were used. All the models were based on the k-ω model. The computational domain extended from 2L in front of the model to 5L behind the model.

While all the models predict the flow to a good extent, the IDDES model gives a slightly greater agreement at the shear layer region for the 35° slant angle. For an angle of 25°, the EARSM model does not register a change in the geometry and the results are similar to those of the previous geometry, i.e., a massive separation. With the hybrid RANS-LES models, the wake is different. Instead of massive separation, only small separations are present. The IDDES model predicts a recirculation bubble, with a reattachment point at X = 168 mm, which is very close to the experimental measurement of Thacker for which the value is X = 160 mm. The DES model observes no recirculation.

EARSM	DES	IDDES	Experiment
0.260	0.316	0.355	0.256

Table 2: 35° slant angle - Drag coefficient

EARSM	DES	IDDES	Experiment
0.280	0.437	0.382	0.384

Table 3:25° slant angle - Drag coefficient

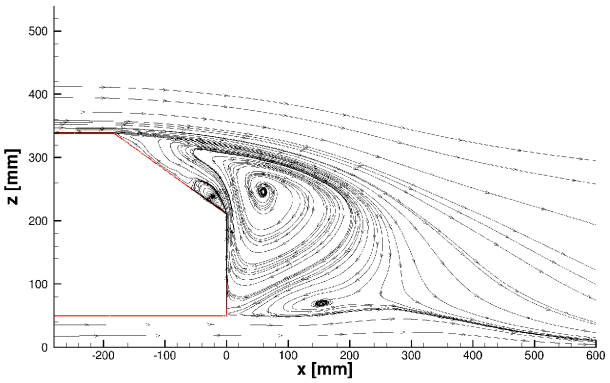

Fig 12: IDDES (avg) flow for 35° slant angle by Guilmineau et al.[6]

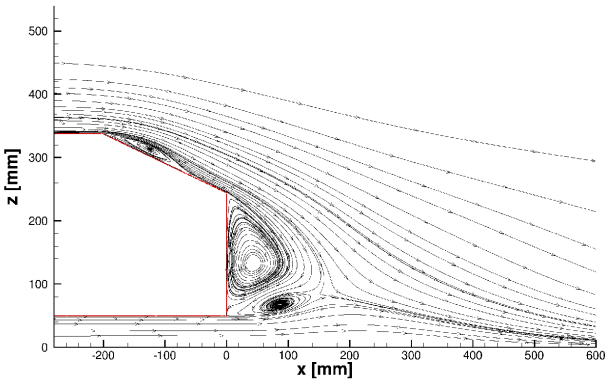

Fig 13: IDDES (avg) flow for 25° slant angle by Guilmineau et al.[6]

Clearly, the IDDES model offers an advantage over the RANS model in terms of the force coefficients and the general flow field, even for the 25° test case. The drag coefficient experiment data refers to the experiments conducted by Linehart et al.[2].

3. Computational Methods

The previous section looked at some of the experiments conducted on the problem and some of the computational approaches used to analyze the problem were also briefly outlined. This section briefly looks into the mathematical formulation of the problem and then describes some of the commonly used computational methods to solve the problem.

3.1 Mathematical Formulation

A. Governing Equations

The governing equation consists of continuity and momentum equations in three dimensions. For the solvers where the assumption of incompressible flow is taken, these can further be simplified.

Continuity equation:

$$\frac{\partial \rho}{\partial t} + \frac{\partial(\rho u)}{\partial x} + \frac{\partial(\rho v)}{\partial y} + \frac{\partial(\rho w)}{\partial z} = 0$$

Navier-Stokes Equations:

$$\frac{\partial(\rho u)}{\partial t} + \nabla(\rho u V) = \frac{\partial p}{\partial x} + \frac{\partial \tau_{xx}}{\partial x} + \frac{\partial \tau_{yx}}{\partial y} + \frac{\partial \tau_{zx}}{\partial z} +$$

$$\frac{\partial(\rho v)}{\partial t} + \nabla(\rho v V) = \frac{\partial p}{\partial y} + \frac{\partial \tau_{yx}}{\partial x} + \frac{\partial \tau_{yy}}{\partial y} + \frac{\partial \tau_{zy}}{\partial z} +$$

$$\frac{\partial(\rho w)}{\partial t} + \nabla(\rho w V) = \frac{\partial p}{\partial z} + \frac{\partial \tau_{zx}}{\partial x} + \frac{\partial \tau_{yz}}{\partial y} + \frac{\partial \tau_{zz}}{\partial z} +$$

B. Problem Assumptions

One of the assumptions is that there is no heat transfer between the flow and the geometry. Air velocity is constant at the inlet section. All the object boundaries will be dealt with as walls with the no-slip shear condition. Because the Mach number is less than 0.3, a lot of studies have also taken the assumption of the flow being incompressible.

C. Boundary Conditions

The following boundary conditions are followed:

- Velocity-inlet: Inlet plane
- Symmetry: Enclosure surfaces
- Walls: Road and object surfaces
- Pressure outlet: Outlet plane

Now, after having formulated the problem mathematically, the next subsection looks at some of the common computational methods used to study the problem, starting with a brief discussion on various models and their effectiveness.

3.2 Turbulence Modeling

It is well-known that the Navier-Stokes equations can describe the unsteady, turbulent flows in the continuum regime. Complex, unsteady turbulent flows can be described using various approximations by certain turbulence models. The key factors which one looks for in a turbulence model are accuracy and computational cost. An optimal combination of these two is necessary for a model to be robust as well as practically viable. The complex dynamic nature of the wake region vortices makes it necessary to model the vortices using temporally and spatially accurate calculations of the flow field using direct numerical simulation (DNS) or large eddy simulation (LES).

DNS explicitly accounts for all scales of motion in a turbulent flow, from the largest to the smallest, and is therefore considered as one of the most accurate turbulent models. But, Kim et al. showed that the DNS of fully developed incompressible channel flow at a Reynolds number of 6000 requires a grid with 2 and 4 million points. This imposes a critical limitation of the applicability of DNS in high Reynolds number flows, and it is impossible to apply DNS for complex 3D turbulent flows using present-day computers.

LES, on the other hand, computes the large-scale structure of turbulent flow directly and the smallest and nearly isotropic eddies are modeled and termed as sub-grid scale eddies. This is achieved by filtering (space averaging) the Navier-Stokes equations to obtain a set of equations that govern the resolved flow. LES is approximately 10 times faster than DNS and is thus used more frequently.

Reynolds Average Navier-Stokes (RANS) is the most practical turbulence handling technique, being less computationally

expensive than LES as well. The dependent variables of the Navier-Stokes equations are decomposed into time-mean and fluctuating parts and the entire equation is time-averaged, which requires an additional set of assumptions.

Detached Eddy Simulation (DES) is a hybrid RANS-LES model which combines RANS and LES to act as a single model, and thus enjoys the computational benefits of RANS and accuracy benefits of LES.

The following subsections give an insight into these turbulence models. It is clear that DNS is not an option as the computational cost of carrying out the simulations is beyond current computational capabilities.

A. Reynolds Averaged Navier-Stokes (RANS)

The time-averaged Navier-Stokes equations have been employed along with approximations based on knowledge of the properties of the problem to give appropriate time-averaged solutions to the Navier-Stokes equations. For stationary incompressible flow (which is the assumed case here), these equations can be written as:

$$\rho\overline{u}_j\frac{\partial\overline{u}_j}{\partial x_j} = \rho\overline{f}_i + \frac{\partial}{\partial x_j}\left[-\overline{p}\delta_{ij} + \mu\left(\frac{\partial\overline{u}_i}{\partial x_j} + \frac{\partial\overline{u}_j}{\partial x_i}\right) - \rho\overline{u'_i u'_j}\right]$$

The last term in the above equation represents the velocity fluctuations (termed Reynolds stress). To obtain equations containing only the mean velocity and pressure, we need to close the RANS equations by modeling the Reynolds stresses as a function of the mean flow. This is known as the closure problem. Several models have been developed to tackle the closure problem, some notable mentions are the Eddy viscosity approach, Prandtl's mixing-length concept, Spalart-Allmaras model, k-ε model, and k-ω model. Most of the previous studies which used RANS for the Ahmed body flow simulation have used the k-ω turbulence model.

The eddy viscosity model (EVM) related the turbulent stresses to the mean flow:

$$-\overline{u'_i u'_j} = \nu_t\left(\frac{\partial\overline{u}_i}{\partial x_j} + \frac{\partial\overline{u}_j}{\partial x_i}\right) - \frac{2}{3}k\delta_{ij}$$

The eddy viscosity $\nu_t = k/\omega$and the evolution of k and ω using the Standard (Wilcox[7]) model is calculated as:

$$\frac{\partial(\rho k)}{\partial t} + \frac{\partial(\rho u_j k)}{\partial x_j} = \rho P - \beta^*\rho\omega k + \frac{\partial}{\partial x_j}\left[\left(\mu + \sigma_k\frac{\rho k}{\omega}\right)\frac{\partial k}{\partial x_j}\right]$$

$$\frac{\partial(\rho\omega)}{\partial t} + \frac{\partial(\rho u_j\omega)}{\partial x_j} = \frac{\alpha\omega}{k}P - \beta^*\rho\omega^2 + \frac{\partial}{\partial x_j}\left[\left(\mu + \sigma_k\frac{\rho k}{\omega}\right)\frac{\partial k}{\partial x_j}\right] + \frac{\rho\sigma_d}{\omega}\frac{\partial k}{\partial x_j}\frac{\partial\omega}{\partial x_j}$$

where $P = \tau_{ij}\frac{\partial u_i}{\partial x_j}$

Using these equations to calculate the eddy viscosity, the RANS based simulations are carried out. The parameters of the k-ω models have to be appropriately set for the solution to converge. The numerical methods for solving RANS equations usually use implicit time-integration schemes like implicit Euler or second-order methods like Crank-Nicolson or three-level methods.

B. Large Eddy Simulations (LES)

The key idea behind LES is the key-filtering of the Navier-Stokes equations for the smallest length scales. An LES filter can be applied to a spatial and temporal field $\Phi(x,t)$ and a spatial filtering operation, a temporal filtering operation or both can be performed. The filtered Navier-Stokes equations can be written as:

$$\frac{\partial \bar{u}_i}{\partial t} + \frac{\partial}{\partial x_j}(\overline{u_i u_j}) = -\frac{1}{\rho}\frac{\partial \bar{p}}{\partial x_i} + 2\nu\frac{\partial}{\partial x_j}\overline{S}_{ij} - \frac{\partial \tau^r_{ij}}{\partial x_j}$$

The Ahmed body is mathematically modeled with a Lagrangian implementation combined with a single linear interpolation shown below:

$$u_i^{n+1}(x = 2l, y, z) = u_i^{n}(x = 2l - U_\infty \Delta t, y, z)$$

The numerical method used to solve the equations is based on a multi-domain Chebyshev-Fourier approximation. The computational domain is decomposed in nonoverlapping subdomains of different lengths depending on the flow region in the streamwise direction. An influence matrix technique is used to ensure continuity. The Gauss-Lobatto-Chebyshev (GLC) mesh is specially adapted when the boundary layer occurs at the boundary of the computational domain. To accumulate the grid point in the vertical direction, a mapping, f:(-1,1) → (0, H) is used, where H represents the channel height.

The equations are solved using a fractional step discretization method. The non-convective terms are handled by using a semi-Lagrangian method and a fourth-order Runge-Kutta scheme. Goda scheme is used to handle the linear viscous term. The divergence-free velocity field is obtained by using a projection step.

LES makes use of an SVV stabilization technique. The SVV term is introduced in the Navier-Stokes equations through an SVV modified viscous term so that the numerical solver solves the semi-discrete system. An operator is defined to refine the mesh around the bluff body, and another one is implemented on the basis of the introduction of SVV modified differentiation matrices.

The Ahmed body is modeled using a volume penalization method in which an additional term is introduced, which approximately cancels the velocity field in the volume of the obstacle. This technique keeps the meshing simple, even in the case of complex geometries, so that very efficient solver can be used. One limitation is that the approximation is no longer spectral locally, but this is not a topic of immediate concern if the mesh cannot resolve the boundary layer. The standard volume penalization method is given by:

$$\frac{\partial u_N}{\partial t} + u_N . \nabla u_N = \; - \nabla p_{N-2} + \nu \Delta_{SVV} u_N - C_\chi(x) u_N$$

where C is the penalization constant and χ(x) is the characteristic function of the obstacle, equal to 1 inside the bluff body and 0 elsewhere.

The near-wall region around the Ahmed body requires particular attention, as it is the main location of turbulence production. A lot of studies used walls functions based on classical log-law profiles to model the viscous sublayer.

Numerical treatment of the near-wall layer is simply based on numerical tests and reasonable arguments, which show that no Gibbs phenomenon occurred in the region, due to the high-frequency dissipation supplied by the SVV term and the O(h) artificial boundary layer. Also, the activation parameter m_n is locally relaxed to keep the global stability of the computation and to capture the actual turbulence production in the best possible manner. This may be formulated as:

$$\frac{\partial u_N}{\partial t} + u_N . \nabla u_N = - \nabla p_{N-2} + \nu \Delta_{SVV} u_N - C_\chi(x) u_N + f_{BL}$$

where $f_{BL} = \chi_{BL}\nu(\Delta^{BL}_{SVV} u_N - \Delta_{SVV} u_N)$

with χ_{BL} equal to 1 in the near-wall region and equal to 0 outside. The operator Δ^{BL}_{SVV} is defined as Δ_{SVV} but makes use of the greater value of m_N. This operator is also anisotropic,

which means that the values of the parameter differ, depending on the direction. The f_{BL} (force term) is treated explicitly, using a second-order Adams-Bashforth extrapolation consistent with the accuracy of the time discretization. The wall coordinates may be estimated using the friction velocity, calculated from the mean flow boundary layer equation.

C. Detached Eddy Simulations (DES)

One of the DES models used for the modeling of Ahmed body flow is the Spalart-Allmaras (S-A) model, which is a one equation RANS model. The S-A turbulent kinematic viscosity is given by:

$$\nu_T = \tilde{\nu} f_{vl}$$

where the following transport equation calculates the variable $\tilde{\nu}$.

$$\frac{D\tilde{\nu}}{Dt} = c_{bl}[1 - f_{t2}]\,\tilde{S}\tilde{\nu} - \left[c_{w1} f_w - \frac{c_{bl}}{\kappa^2} f_{t2}\right]\left[\frac{\tilde{\nu}}{d}\right]^2 + \frac{1}{\sigma}\left[\nabla.((\nu + \tilde{\nu})\nabla\tilde{\nu}) + c_{b2}(\nabla\tilde{\nu})^2\right] + f_{t1}\Delta U^2$$

The constants and the production term $\tilde{S}$ is appropriately defined, with S being the magnitude of the vorticity. For the Ahmed body case, this equation reduces to:

$$\frac{D\tilde{\nu}}{Dt} = c_{bl}\tilde{S}\tilde{\nu} - \left[c_{w1} f_w\right]\left[\frac{\tilde{\nu}}{d}\right]^2 + \frac{1}{\sigma}\left[\nabla.((\nu + \tilde{\nu})\nabla\tilde{\nu}) + c_{b2}(\nabla\tilde{\nu})^2\right]$$

The detached eddy simulation is a 3-D unsteady numerical model which functions as a subgrid-scale model in regions where grid density is fine enough for an LES (largely separated zones away from the walls, for resolving 3-D eddies which are geometry dependent), and as a RANS model in regions where it is not (for flow in thin shear layers near the wall surfaces). The distance to the nearest wall is defined as the minimum of the actual distance and a constant times the largest distance between the cell center under consideration and the cell center of the neighbors. Mathematically,

$$\tilde{d} = min(d_w, C_{DES}\Delta)$$

where $\Delta = max(\Delta x, \Delta y, \Delta z)$

A model inside the whole attached boundary layer as streamwise or spanwise or both grid spacing parallel to the wall are at least on the order of the boundary layer thickness, and thus $\tilde{d} = d_w$ and the model works as a standard S-A RANS turbulence model inside the boundary layer. In regions far from the wall, $d_w > C_{DES}\Delta$ and thus the length scale of the model becomes grid-dependent, and the model performs as a subgrid-scale version of the S-A model for eddy viscosity.

The numerical modeling involves implicit time stepping and discretization, and hence a cell-centered, finite-volume approach is used. The flow solution algorithm comprises of the following five fundamental tasks -

- Construction of initial conditions for the Reimann problem at any face
- A solution of the Reimann problem
- Construction of viscous fluxes at any given face
- Time integration
- Boundary conditions

The first step is critical to the algorithm, for it includes any limiting or dissipation and it largely determines the spatial accuracy and truncation error. This is done with the help of discretization, which is able to achieve second-order time accuracy during numerical simulations.

D. Improved Delay Detached Eddy Simulations (IDDES)

Another version of DES used for the problem is IDDES which combines DES and wall-modeled LES. It looks after several shortcomings like a log-layer mismatch, grid-induced separation, etc. For a study that compared some of the turbulent models, IDDES performed the best for the rear base slant angle below as well as above the critical separation angle.

IDDES can be constructed by modifying the destruction term of the turbulent kinetic energy (TKE) term by explicitly introducing a length scale, L_{IDDES}.

$$\frac{\partial(\rho k)}{\partial t} + \frac{\partial(\rho u_j k)}{\partial x_j} = \widetilde{P}_k - \frac{\rho k^{3/2}}{L_{IDDES}} + \frac{\partial}{\partial x_j}\left[\left(\mu + \sigma_k \mu_t\right)\frac{\partial k}{\partial x_j}\right]$$

where k is the modeled TKE, and L_{IDDES} is introduced as,

$$L_{IDDES} = \widetilde{f}_d(1 + f_e)L_{RANS} + (1 - \widetilde{f}_a)L_{LES}$$

with $L_{RANS} = k^{0.5}/(\beta^* \omega)$ and $L_{LES} = C_{DES}\Delta$.

The function $\widetilde{f}_a$ is defined as $max[(1 - f_{dt}), f_B]$, which is determined by the geometry dependent part f_B and flow-dependent part f_{dt}. For $f_e = 0$, the IDDES equations revert back to DDES and for $f_e > 0$ and $\widetilde{f}_{dl} = f_B$, IDDES acts as LES near the wall.

4. Conclusions

The Ahmed body problem is a simplified representative model of real-world automobiles, specifically aimed at observing some interesting phenomenons that occur in the wake region of a car. The study by ICCT (section 1.4) makes it clear that the aerodynamic drag works as a deciding factor for the total power consumption of the vehicle and needs to be dealt with seriously. The proper study of flow over car models led to better and more efficient designing of vehicles. While the model is not that complex, still it captures some of the amazing phenomena which occur, e.g., the flow separation in the wake region with the rear base slant angle of 30° as a critical angle.

The experiments not only provided these useful insights into the problem but also provided valuable data for using computational methods to model and simulate the flow. The computational methods help in understanding the system better and also tells us more about the nature of turbulent flows, which are still a mystery (not completely) to mankind.

Recent advances in computational power have enabled us to carry out more complex and costly computational studies. Currently, IDDES is one of the most promising approaches for the problem and resembles the experimental results very well. More research using this model might lead to more precise insights about the nature of the flow.

The problem is still open and in search of better and better models which can perfectly explain the turbulent flow nature. DNS, a really accurate approach cannot be applied to the problem due to computational limitations right now, which might also be tackled in the upcoming years and will open new approaches to the problem.

5. References

[1] Ahmed SR, Ramm G and Faltin G 1984 *Some Salient Features of the time-averaged ground vehicle wake*

[2] Lienhart H, Stoots C, and Becker S *Flow and Turbulent Structures in the Wake of a Simplified Car Model (Ahmed Body)*
[3] Gillieron P and Chometon F 1999 *Modeling of stationary three-dimensional separated flows around an Ahmed reference model*
[4] Howard R J A and Pourquie M 2002 *Large eddy simulation of an Ahmed reference model*
[5] Kapadia S and Roy S 2003 *Detached Eddy Simulation Over a Reference Ahmed Car Model*
[6] Guilmineau E et al. 2016 *Assessment of RANS and DES methods for the Ahmed Body*
[7] Xiao Z and Luo K *Improved delayed detached-eddy simulation of massive separation around triple cylinders*
[8] Tennekes H and Lumley J L 1994 *A First Course in Turbulence*
[9] https://en.wikipedia.org/wiki/Turbulence and related articles